EFDA–JET–PR(13)15

S.N. Gerasimov, T.C. Hender, J. Morris, V. Riccardo, L.E. Zakharov
and JET EFDA contributors

Plasma Current Asymmetries During Disruptions in JET

Plasma Current Asymmetries During Disruptions in JET

S.N. Gerasimov[1], T.C. Hender[1], J. Morris[1], V. Riccardo[1], L.E. Zakharov[2]
and JET EFDA contributors*

JET-EFDA, Culham Science Centre, OX14 3DB, Abingdon, UK

[1]EURATOM/CCFE Fusion Association, Culham Science Centre, OX14 3DB, Abingdon, UK
[2]Princeton Plasma Physics Laboratory P.O. Box 451. Princeton, New Jersey, USA
** See annex of F. Romanelli et al, "Overview of JET Results",*
(24th IAEA Fusion Energy Conference, San Diego, USA (2012)).

Preprint of Paper to be submitted for publication in
Nuclear Fusion

ABSTRACT

A key feature of disruptions during Vertical Displacement Events (VDEs) in JET is the long lasting toroidal variation in the measured plasma currents, i.e. the plasma current asymmetries. The unique magnetic diagnostics at JET (either 2 toroidal opposite or 4 toroidal orthogonal locations) allow for a comprehensive statistical analysis of asymmetrical disruptions with a large scale database. This paper presents analysis of 4854 disruptions over an 18 year period that includes both the JET carbon (C) wall and the ITER-Like (IL) wall (a mixed beryllium/tungsten first wall). In spite of the I_p quench time significantly increasing for IL-wall compared to C-wall disruptions, the observed toroidal asymmetry time integral (~ sideways force impulse), did not increase for IL-wall disruptions. The I_p asymmetry is found to have a dominantly m=n=1 structure and rotates with a sporadic behaviour, in general. The distributions of the number of rotation periods are found to be very similar for both C- and IL-wall disruptions, and multi-turn mode rotation was sometimes observed. The I_p asymmetry amplitude has no degradation with mode rotation frequency for both the C- and IL-wall disruption data, and therefore dynamic amplification remains a potentially serious issue for ITER due to possible mechanical resonance of the machine components with the rotating asymmetry.

1. INTRODUCTION

Disruptions remain an essential issue for any scenario operation of ITER [1]. The electro-magnetic and heat loads, and runaway electron generation are the main concerns of the disruption impacts on the machine components [2]. Toroidal asymmetries in the measured plasma currents (I_p) and first plasma current moments ($M_{IZ} = \int Z J_\phi dRdZ$ and $M_{IR} = \int R J_\phi dRdZ$) have been observed in JET during Vertical Displacement Events (VDEs), which can lead to substantial sideways forces of up to about 4 MN [3], [4], [5], [6], this in turn causes significant displacements of the JET torus [3]. These "VDE" forces increase for larger machines such as ITER. The sideways force F_x and vertical force F_z on the vessel are expected to be an order of magnitude larger in ITER in comparison with JET [5], [7], [8], this follows from simple dimensional analysis: $F_x \propto B_T I_p a$, $F_x^{ITER} \cong 2 \cdot 5 \cdot 2 F_x^{JET} \cong 20 F_x^{JET}$; $F_z \propto I_p^2 R$, $F_z^{ITER} \cong 25 \cdot 2 F_z^{JET} \cong 50 F_z^{JET}$, where B_T, I_p, a are toroidal field, plasma current and minor plasma radius, respectively. (This assumes that JET and ITER have similar plasma shape, plasma profiles, mode structure and relative asymmetry amplitude). Detailed engineering analysis confirms the order of magnitude increase of these forces for ITER [8]. Apart from the force itself, the force impulse ($\int F_z \, dt$) and force time behaviour are important for the vessel structural loads. The rotation of toroidal asymmetrical currents during disruptions was observed on JT60-U [9], Alcator C-Mod [10], DIII-D [11] and later on JET [5], [12], ASDEX-U [13] and NSTX [14]. The frequencies that are close to the structural natural frequencies of the machine components can cause major dynamic amplifications of the loads. For the ITER vessel the most problematic rotation frequency is ~3-8 Hz, which is the range of the fundamental mechanical vessel frequencies [15].

In order to better to understand the sideways forces one has to understand what physics lead to

the plasma current asymmetries. The observed I_p asymmetries have been interpreted as a kink mode $m=n=1$, when the plasma boundary q-value decreases to about 1 to permit kink instability [3]. The nature of kink mode can explain the origin of the toroidal plasma current asymmetries. Considering a cylindrical plasma, with circular cross-section, in a strong (equivalent to toroidal field in torus geometry) magnetic field and plasma current (I_p) along the cylinder Z axis, see Fig.1a. Allowing a kink mode deforms the straight cylindrical plasma to a helical structure. This helical deformation evokes surfaces plasma currents to eliminate the normal component of the magnetic field on the plasma surfaces. The bulged outer surface always carries the negative current, opposite to I_p, whereas the bulged inner surface always carries the positive current.

However, the existence of the long lasting kink mode $m=n=1$ contradicts the traditional interpretation of the global kink mode behaviour [16]. A modern physically rooted model has been proposed based on the helical surface currents that occur in the $m=n=1$ kink mode [17]. The helical surface currents (named Hiro currents in [17]) which are assumed to flow into the wall when the kinking of the plasma surface causes it to touch the wall, see Fig. 1b. The model likely underlies the appearance of the I_p asymmetries and halo current asymmetries [7]; as discussed below the relative directions of the plasma motion and observed wall currents fits this model. On the other hand, an empirical source and sink model has been proposed that explains the observed I_p asymmetries [4] and forces inferred from the vessel motion. This model has been used to calculate the structural loads from I_p asymmetries in ITER [8].

JET magnetic diagnostics, which are essential for the presented results, are described in section 2. The procedures used to design plasma current asymmetry database are given in section 3. The observed during VDEs $m=n=1$ mode structure is outlined in section 4. The plasma current asymmetries, sideways forces and impulses data, which was extracted from 4854 disruptions over an 18 year period of JET operation, is detailed in section 5. The plasma current asymmetries rotation is discussed in section 6. The remaining issues, which will be subject of future investigations, are conferred in section 7. The results of the performed disruption analyses in term of plasma current asymmetries are summarized in section 8.

2. DIAGNOSTICS

On JET the toroidal asymmetries of the plasma current (I_p) and M_{IZ} and M_{IR} moments are measured using arrays of in-vessel poloidal pick-up coils (named Internal Discrete Coils, IDC) and ex-vessel saddle loops at 4 orthogonal toroidal locations (see Fig.2). Each octant is equipped with 18 pick-up coils and 14 saddle loops.

The plasma current is calculated using the following equation:

$$I_p = \frac{1}{\mu_0}\sum_{i=1}^{4} B_{\vartheta i} d_i - \sum_{i=1}^{4} n_{Di} I_{Di} - (I_{RRU} + I_{RRL}), \qquad (1)$$

where $B_{\vartheta i}$ is the poloidal (tangential) field measured by IDC with index "i", d_i is the length of

the relevant arc. The last two terms are the axisymmetric currents occurring inside the measuring contour, where $\sum_{i=1}^{4} n_{Di} I_{Di}$ are the currents in divertor poloidal field (PF) coils and ($I_{RRU} + I_{RRL}$) are the currents in the restraining rings: they are identical for all octants. Equation (1) does not include the axisymmetric currents in the divertor support structure and divertor PF coil cases (I_{MK2}) because reliable measurements are not available for all the pulses in the presented database. The amplitude of the induced I_{MK2} could be up to 5% of pre-disruptive plasma current for fast CQ. Nevertheless, ignoring the axisymmetric I_{MK2} current does not affect the toroidally asymmetrical part of the plasma current.

Figure 3 illustrates the nature of the measured I_p asymmetries. Supposing the plasma is touching the wall in octant 7, during the kink mode m=n=1 instability, a negative plasma surface current flows in the vessel in octant 7 and bypasses the contour of B_ϑ integration. In the opposite octant 3, the I_p diagnostic measures the total plasma current, as the plasma does not touch the wall.

The first plasma current vertical moment is calculated using the equation:

$$M_{IZ} = \frac{1}{\mu_0}\left(\sum_{i=1}^{18} B_{\vartheta i} z_i d_i + \frac{1}{2\pi}\sum_{i=1}^{14} \Psi_i \ln\left(\frac{R_o}{r_i}\right)\right) - \sum_{i=1}^{4} z_{Di} n_{Di} I_{Di} - (z_{RRU} I_{RRU} + z_{RRL} I_{RRL}), \qquad (2)$$

where Ψ_i is the flux measured by Saddles with index "i", z_i and r_i are IDCs and Saddle coil coordinates, z_{Di} and $z_{RRU/L}$ are divertor coil and restraining ring coordinates respectively. The divertor support structure and divertor PF coil contributions were not taken into account in equation (2), see previous explanation for equation (1). It is worth mentioning that the current centroid position does not reflect the true geometrical plasma boundary position in the case of asymmetrical surface currents.

The pick-up coil and saddle signals are processed by analogue low-drift integrators with a 16-bit analogue to digital converter. The data is recorded at a 5kHz sampling rate during the whole JET pulse or, at least, during the disruption time window. Data for octants 3 & 7 has been recorded from Pulse No: 32102 (15/10/1994) onwards. Additionally two octants 1 & 5 have been recorded regularly from Pulse No: 64329 (03/11/2005) onwards, allowing mode amplitude and phase to be deduced.

All 8 JET octants were originally equipped with identical sets of IDCs and Saddles (with some minor exceptions for 3 and 7 octants). Later on, the 9 upper IDCs were removed from octant 8 to allow the installation of another diagnostic.

There are two toroidal in-vessel passive structures, which can affect the interpretation of the IDCs measurements. They are the restraining rings and the divertor support structure/divertor coil cases, Fig.3. Two of the IDCs (8 and 11 coils) are located between the vessel and restraining rings. So the vessel current can flow through the restraining rings and affect coil 8 and 11 local measurements. Coil 8 and 11 are effectively located outside the vessel current circuit while the rest of the coils (apart of bottom coils, see comments below) are located inside the vessel current circuit. Fig.4 shows the poloidal field subtracted on 2 opposite sides of the torus (octant 7 – octant

3), during an upward VDE. The change of sign of the poloidal field in Fig. 4, with time, is due to rotation of the I_p asymmetry. It can be seen by inspection that the field at coil 8 has an opposite sign to that expected by simple interpolation between coils 7 and 9, and likewise for coil 11. It is thought this change in sign is caused by currents flowing in the vessel restraining ring, between the coil and plasma. To assess the impact of this on the deduced plasma current, the signal in coil 8 has been replaced by an average of the signals from coils 7 and 9, and the coil 11 signal has been replaced by an average of coil 10 and 12. This procedure indicates that the shielding effect produces up to a ~15% underestimate of the asymmetric current and vertical moment calculated by (1) and (2). At least three IDCs (13, 14 and 15 coils) are positioned between the vessel and divertor passive structure. Hence, for downward VDEs the magnetic measurement interpretation suffers due to the uncertainty of the current passive structure circuits.

3. PLASMA CURRENT ASYMMETRY DISRUPTION DATABASE

The presented JET disruption database includes pulses, where $I_p^{dis} > 1.0$ MA (I_p^{dis} is pre-disruptive plasma current, defined as the average I_p over 20-50 ms before the disruption time, T_{dis}), for all cases, not just VDEs. In the results presented the time of disruption is defined as the moment when $|dIp/dt| > 25$MA/s for at least 2 ms or as the time of the peak of the voltage loop spike (> 10 V). Manual checks and minor corrections (where necessary) were applied to the entire database. Some of the disruptions exhibit multiple plasma current spikes, where the first event is treated as the start of the disruption. The above algorithm provides a disruption time just before the plasma current spike followed by plasma current quench (CQ) or a disruption time just before plasma current quench for VDE disruptions. Nevertheless, the plasma current asymmetry analysis is not affected by the somewhat arbitrary choice of the disruption time.

The database includes 4854 (unplanned and intentional, as part of disruption study) disruptions in the range Pulse No's: 32102 - 83794, which covers a period of JET operation from 15/10/1994 to 27/07/2012. During this period, 1300 disruptions have been recorded using 4 octants, which have been used for mode rotation analysis. The pre-disruptive plasma current and toroidal field are in the range (1.0-4.6)MA and (0.6-3.8)T respectively for the entire database.

Replacement of carbon plasma-facing components (referred to here as JET "C-wall") by solid beryllium limiters and beryllium tiles in the main chamber, and a combination of bulk W and W-coated divertor tiles (referred to here as JET "IL-wall") was completed on JET in 2011 [18], [19], [20], [21]. The presented C-wall I_p asymmetries rotation (4 octants) database contains 951 shots. The C-wall database also contains 3490 pulses of two-octant disruption data, which has been used for non-rotational analysis only. The whole IL-wall current database contains 413 disruptions out of which 349 are recorded using 4 octants and 64 are recorded in 2 octants only because of the Data Acquisition System (DAS) faults or insufficient duration of the 5 kHz window in one of the magnetics DAS. Figure 5 shows the waveforms of the typical asymmetrical VDE disruption before and during a plasma current quench, where plasma current asymmetries are $\Delta I_{p73} = I_{p7}\, I_{p3}$

and $\Delta I_{p51} = I_{p5} I_{p1}$ with I_{p1} = octant 1 plasma current etc. In the limited number of cases examined, the I_p asymmetries usually appear when the q safety factor drops to 1 because of the large plasma vertical displacement during VDE causes the minor plasma radius decrease at approximately constant I_p.

The amplitude of the plasma current asymmetries is calculated as $\sqrt{(I_{p7} - I_{p3})^2 + (I_{p5} - I_{p1})^2}$. In the case when only the two-octant measurements were available the amplitude plasma current asymmetries were calculated as $I_p^{asym} = \sqrt{(I_{p7} - I_{p3})^2}$ or $I_p^{asym} = \sqrt{(I_{p5} - I_{p5})^2}$ [5]. The other quantity which has been used, is the normalised amplitude $A_p^{asym} = I_p^{asym} / |I_p^{dis}|$. To avoid noise contributing to the results, A_p^{asym} quantity is evaluated for times when the start and end time window satisfied the following conditions: $A_p^{asym} > 0.5\%$, $|I_p| > 0.1|I_p^{dis}|$ and $|I_p^{asym}| > 20$kA for the first and last 1 ms window in order to disregard short-lived spikes. The A_p^{asym} values do not satisfy the criteria are treated as a "noise" and forced to zero. The above defined time window was applied for all other waveforms, which have been used for analysis.

Under the previously developed ITER specification [24] a +/-2 ms triangular smoothing of the JET data was applied, on the basis that such short timescale behaviour (when extrapolated to ITER) will have no mechanical effects. Given the ~3-8 Hz ITER vessel frequency the choice of +/-2 ms smoothing time (though somewhat arbitrary) is conservative. The quantities such as the maximum in this paper were chosen from the smoothed waveforms to ignore the short-lived outliers. Figure 6 shows an example of the plasma current asymmetries at the different stages of the numerical processing: I_p^{asym} - amplitude of the asymmetries (peak to peak, original and then trimmed), A_p^{asym} - normalized asymmetry amplitude (trimmed and smoothed).

The peak values of A_p^{asym}, extracted from smoothed waveforms, are plotted in Fig. 7. The 4-octant data presents the true magnitude of the asymmetries. On the other hand two octant data, in general, can underestimate the amplitude for asymmetries which are orthogonal to diagnostics. The fractions on the figure indicate the share of the disruptions that are treated as asymmetrical disruptions; only the asymmetrical disruptions are plotted. The rest of the disruptions are treated as symmetrical disruptions because the level of asymmetry is below the "noise" level. The total fraction of asymmetrical disruptions in the presented database is 0.41 = 2003/4854, where C-wall asymmetrical disruption fraction is 0.40 = 1771/4441 and IL-wall fraction is 0.56 = 232/413. The boundary of the normalised I_p asymmetries $A_p^{asym} \approx 17\%$ is about the same for whole range of 4854 disruptions.

To systematically quantify the magnitude of I_p asymmetries the integral $A = \int A_p^{asym} dt$ has been used. Ignoring transients then $A \sim \int F_x dt / I_p B_t a$, where F_x is the asymmetric (or sideways) force. So A is related to the magnitude of the sideways force impulse; it should be noted that A represents the modulus of the impulse and not a projection in a specific direction. Of the asymmetrical disruptions, the majority (76%) are upward going VDEs. Moreover, of the most severe observed asymmetrical disruptions ($A > 0.2A_{max}$), almost all disruptions (99%) are upward going VDEs.

4. I_P ASYMMETRY STRUCTURE

As discussed in detail below (Section 6) the I_p asymmetry structure can rotate toroidally. This rotation allows one to examine the spatial structure of the asymmetry. Figure 8 shows the poloidal field waveforms around the torus: $\widetilde{B}_p(i,j) = B_p(i,j) - \langle B_p(i)\rangle$, where $B_p(i,j)$ is the poloidal field at i-coil and j-octant, $\langle B_p(i)\rangle$is an average for four octants. The change of the $\widetilde{B}_p$ poloidal field with time, is due to the rotation of the asymmetric component of the plasma current, and can be seen to have an $n = 1$ toroidal mode structure. Likewise Fig. 9 shows the poloidal variation of $\widetilde{B}_p(i,j)$ at octant 3. The variation of poloidal mode structure can be seen to be dominantly $m = 1$, though the variation is far from uniform with poloidal angle. As with the pulse shown in Fig.5, equilibrium reconstructions show that edge-$q \sim 1$ at the time when the I_p asymmetries start. The picture is thus consistent with an $m = n = 1$ kink mode causing the observed wall current asymmetries.

The phase relationship of the measured I_p and first vertical plasma current moment (M_{IZ}) is a discriminator for models of the wall currents. Figure 10 shows the typical waveforms (I_p, ΔI_p, ΔM_{IZ} and ΔZ) during the plasma current quench. The measured absolute magnitude of the plasma current is greater when displacement is also greater [3], [4], [5]. Specifically, the toroidal asymmetry in plasma currents corresponds to negative currents (relative to the direction of plasma current) flowing in the vessel as shown by the I_p and M_{IZ} asymmetries phase diagram (Fig.11). The fractions in Fig.11 present the share of the disruptions which were used for the plot. The remainder of the disruptions were below "noise" level (see previous definition for "noise"). The sign of the observed asymmetry corresponds to the predictions of the Wall Touching Kink Mode theory [7], [17] as well as to simulations with the M3D code [22].

5. PLASMA CURRENT ASYMMETRIES, SIDEWAYS FORCES AND IMPULSES

The variation of A (A_{4oct} *or* A_{2oct}) = $A_p^{asym}\,dt$ over the disruption database is plotted in Fig. 12. In cases where only two opposite octant data values were available then a 2-octant asymmetry was defined assuming a pure sine wave in time $A = \pi A_{2oct}/2$ (generally $\pi A_{2oct}/2$ gives a good approximation of the 4-octant data). This is shown in Fig. 13, where for shots with 4 octant data the value of A_{4oct} is compared against $\pi A_{2oct}/2$. It can be seen that on average $\pi A_{2oct}/2$ is a good approximation, however A_p^{asym} does not vary sinusoidally in general and so there is some scatter. The probability that a certain value of A is reached can be inferred from Fig.14. The largest I_p asymmetries correspond to upward moving VDEs – quantified by A the largest 17.6% are all upward going VDEs. All the specific time histories of pulses shown in this paper are for upward moving VDEs.

The database contains results for the C-wall and IL-wall - it is known that the wall material strongly affects the disruption due to impurity radiation during the current quench [25], [26], [27]. There is a significant difference in the current decay for C-wall and IL-wall disruptions. In Fig.15 the normalized plasma current for all IL-wall disruptions (Fig. 15a) and for C-wall disruptions (Fig.15b presents subset of 951 C-wall disruptions before IL-wall installation, 4-octant recorded)

shows substantially longer current quench times for the disruption with the IL-wall. The entire disruption database demonstrates that the CQ time distribution for IL-wall is broader and generally shifted to longer decay times in comparison with C-wall [12], see Fig. 15c. Moreover, a large fraction of IL-wall disruptions last for hundreds of milliseconds. This occurs because the current quench duration relates to the L/R (inductance/resistance) time of the plasma, and hence the IL-wall plasma temperature which is higher than for C-wall disruptions due to the absence of carbon [18], [23]. The CQ time is also affected by VDE dynamic.

Despite the longer IL-wall CQ times the sideways impulse measured by A does not increase. This is illustrated in Fig. 16 which shows that IL-wall I_p asymmetry data points are inside the C-wall domain. The data boundaries for the whole current quench duration are:•

- $A = 0.10\tau_{80\text{-}20}$ with A_{max} = 3.5ms on the C-wall data (green lines);
- $A = 0.06\tau_{80\text{-}20}$ with A_{max} = 2.0ms on the IL-wall data (magenta lines).

It is thought that a comparison of IL-wall data should be done with recent C-wall data because of the JET power supply upgrade, improvement of discharge shutdown etc. The recent C-wall disruptions (4 octant data, pulses in the range 64329 – 79831) and the IL-wall data have about the same boundary (magenta lines on the Fig.16). The average CQ duration for two thresholds of the I_p asymmetries presented below:

	$A > 1$ms	$A > 0.5$ms
IL-wall	56.1ms	54.0ms
C-wall, from Pulse No: 64329 onwards	30.0ms	28.0ms
C-wall, whole database	41.7ms	39.3ms

It can be seen that the severest asymmetries have an average CQ duration two times longer for IL-walls in comparison with C-wall disruptions (from Pulse No: 64329 onwards).

In an integral sense these values of A_{max} give the bounding values, however if a trapezoidal envelope for A_p^{sym} is fitted then larger values are needed; the traces of A_p^{sym} for the C-wall and IL-wall disruptions with largest values of A (A_{4oct} or A_{4oct}) are shown in Fig.17, Fig.18 and Fig.19. Fig.17 and Fig.19 present the severest disruptions from the whole C-wall and IL-wall data, respectively. Fig.18shows recent C-wall 4 octant data. In these plots t = 0 is defined such that $\int_{t<0} I_p^{asym}\,dt = \int_{t>0} I_p^{asym}\,dt$. As can be seen by visual inspection the trapezoidal envelope with an area of 3.5 ms, does not bound the observed A_p^{sym} waveforms, Fig. 17 and Fig. 18. A conservative choice would be 4.4 ms and a very conservative choice would be 6.3 ms for C-wall disruptions. The IL-wall disruptions are also well bounded by C-wall disruption envelopes, Fig. 19. The scaling of the JET plasma current asymmetry data to ITER was discussed in [8].

The sideways force can be evaluated using Noll's formula [3], $F_x^{Noll} = {}^{\pi}/_{2}\, B_T \Delta M_{IZ}$, which gives the upper estimation for sideways force [17]. The advantage of the Noll's formula is that it includes quantities which are directly measured by magnetic diagnostics, see for example Fig.20. Both quantities, I_p^{asym} and $F_x^{Noll} = {}^{\pi}/_{2}\, B_T \Delta M_{IZ} \propto B_T I_p^{asym} a$, can be used to characterise peak loads during

asymmetrical disruptions. Figure 21 shows the variation of the sideways force impulse evaluated using Noll's formula $Imp^F = \int F_x^{Noll}\, dt$ for the disruption database, where F_x^{Noll} is the force modules. The sideways force impulse can also be deduced from the plasma current asymmetry: $Imp^A = \pi B_T \langle a \rangle \int I_p^{asym}\, dt = \pi B_T \langle a \rangle \int I_p^{dis} A$, where $\langle a \rangle$ is the average plasma minor radius. The plasma minor radius was taken from EFIT reconstruction just before disruption in the time window $[T_{dis} - 0.1\text{s}: T_{dis}]$ or was taken as $\langle a \rangle$ =1.205m (average data) if EFIT data was not available before disruption. Again, the two-octant data was multiplied by a factor $\pi/2$ assuming a pure sine wave rotation in time. Both evaluations of sideways impulse produce similar results, see Fig. 22.

It should be noted that since the asymmetry can rotate (see section 6) there is no direct relationship between the magnitude of the sideways impulse A (or Imp^F) and the ensuing sideways displacement of the vacuum vessel in general. There are three possible types of rotations: trapped mode, non-resonant and resonant rotations. For example, provided it is not near a resonant frequency of the vessel, a rotating asymmetry will produce less sideways displacement than a non-rotating asymmetry.

6. THE ROTATION OF PLASMA CURRENT ASYMMETRIES DURING DISRUPTIONS IN JET

6.1 ROTATION NUMBERS

The I_p asymmetry rotation is important since it can lead to the dynamic amplification of the applied force if resonance with the vessel or an in-vessel component occurs. In general for JET the duration of the mode rotation is short compared to resonance periods of the vessel etc (~14-17 Hz [28]), and so dynamic amplification is not an issue. However in ITER the situation can be reversed (duration mode rotation > mechanical resonance periods) making this an issue [15].

The I_p asymmetry rotation shows significant scatter in magnitude, frequency and direction [5], [12]. The 4-octant JET magnetic diagnostics allow the extraction of reliable information about mode toroidal rotation during disruptions. Figures 23, 24 and 25 show the asymmetrical disruption waveforms and the traces of the tip of vector $\delta I_p(t) = (\delta I_{51}(t)\,\vec{e}_x + \delta I_{73}(t)\vec{e}_y)/I_p^{dis}$ for discharges with differing rotation behaviour. It can be seen that the rotation is highly variable and it is found that neighbouring pulses (which are otherwise similar) show sometimes similar and sometimes very different rotation behaviour, Fig.26. Nevertheless the neighbouring pulses with similar asymmetry amplitude behaviour show similar rotation behaviour as well, see traces for Pulse No's: 70236 and 70238 shots on Fig.26. However, at the present there is no complete understanding of the rotational physics or appropriate scaling, though a model has been proposed [29].

Statistical analysis of the rotation behaviour requires the use of criteria to extract a subset to avoid noise polluting the results; only shots satisfying $A = \int A_p^{asym}\, dt > 0.5ms$ condition have been used for the rotation statistical analysis. So the rotational statistic has been reduced from 951 to 155 shots for C-wall and from 349 to 88 shots for IL-wall. The number of rotations during disruption was defined as $N = (\varphi_{max} - \varphi_{min})/2\pi$. The N distributions are very similar for C- and

IL- walls. However the mode rotation slightly increased for the IL-wall $\mu^N_{IL} = 2.1$ $\sigma^N_{IL} = 1.2$) in comparison with the C-wall $\mu^N_C = 1.6$ ($\sigma^N_C = 0.8$), Fig.27. The rotation of the I_p asymmetry can be in either direction but it is most commonly seen in the electron direction (i.e. opposite to the plasma current direction) [12].

6.2 ROTATION FREQUENCIES

An additional constraint has been applied for statistical analysis of the observed frequencies - analysis was only performed for pulses where the rotation exceeded one full turn during the disruption. As a result of this constraint, the total number of the shots analysed for their frequency behaviour was reduced to 103 shots for C-wall and to 73 shots for IL-wall. The rotation frequency, presented in the current analysis, has been calculated as $f = 1/\tau$, where τ is the one turn period. The average $\langle A_p^{asym} \rangle$ plasma current asymmetry amplitude has been calculated during the one period of rotation used to evaluate f. The above described algorithm has been applied to C- and IL- walls disruptions independently.

Following this the data points were divided into five $\langle A_p^{asym} \rangle$ regions: $\langle A_p^{asym} \rangle < 2\%$, $2\% \le \langle A_p^{asym} \rangle < 4\%$, $4\% \le \langle A_p^{asym} \rangle < 6\%$, $6\% \le \langle A_p^{asym} \rangle < 8\%$, $\langle A_p^{asym} \rangle \ge 8\%$. The means and the standard deviations of the distributions were calculated and plotted in Fig.28, where it can be seen that the rotation frequency does not decrease with mode amplitude.

7. OUTSTANDING ISSUES

As discussed above the plasma current asymmetries are dominantly $m = n = 1$ mode, and so the vertical and radial displacements (i.e. mode amplitude) of the plasma boundary would be expected to be approximately equal. However, the magnetic diagnostic show a lower first radial plasma current moment variation (ΔM_{IR}) compared with ΔM_{IZ}, Fig.29. It is possible that the radial current centroid position measurements are strongly affected by surface currents and do not reflect the true geometrical plasma boundary position in the case of $m = n = 1$ mode during the plasma CQ.

For the accurate calculation of the sideways forces, an appropriate wall model linked to kink mode evolution is needed. Together with a simple adiabatic shrinking of the plasma cross-section, this would automatically determine the evolution of mode amplitude as well as the forces. This is not available today, nor is it expected to be available in the near future.

The relationship of the poloidal halo current asymmetry to the I_p asymmetry in JET is discussed elsewhere [30], [31]. There is a strong correlation but there is not a simple proportionality relationship. There is a correlation between the I_p asymmetry and halo asymmetry, though with a large spread [31]. This issue needs further investigation.

SUMMARY AND DISCUSSION

The JET disruption data shows toroidal asymmetries in I_p that can translate into substantial sideways forces on the vacuum vessel. These asymmetries have a dominantly $m = n = 1$ structure,

and can be interpreted as arising from a $m=n=1$ kink mode.

The present JET database includes 4854 disruptions over an 18 year period. For fairly recent shots around 1300 are available with data in 4 toroidally orthogonal octants, allowing the phase and amplitude to be deduced. Previously only 2 toroidally opposite octants of data were regularly recorded. The amplitude (smoothed, peak to peak) of the I_p asymmetries is ≤ 17 % of pre-disruptive I_p; and the severest asymmetries have an average CQ duration of ~30 ms for C-wall disruptions (from #64329 onwards) and two times longer for IL-walls. The plasma current quench time is significantly increased for IL-wall compared with C-wall disruptions. In spite of this, the observed I_p toroidal asymmetry time integral, A (~ sideways force impulse), did not increase for IL-wall disruptions and remained inside the C-wall data domain that is 3.5 ms. Due to the observed I_p toroidal asymmetry rotation which occurs for some pulses, the sideways displacement cannot be directly linked with the magnitude of the sideways impulse (A) – the relationship of the I_p asymmetries and sideways vessel displacements will be the subject of a future publication.
Taking a trapezoidal shaped envelope, one with 3.5 ms area does not contain all of the observed waveforms. A conservative choice would be 4.4 ms and a very conservative choice would be 6.3 ms for C- and IL-wall disruptions.

Although not discussed in this paper, the effect of Massive Gas Injection (MGI) on the I_p asymmetries has been examined [23]. It is found the MGI reduces the I_p asymmetries by an order of magnitude, substantially ameliorating the problem.

The rotation of the I_p asymmetry during the I_p quench has a quite variable behaviour and is not reproducible on a shot-by-shot basis. There is no confirmed understanding of the rotational physics or appropriate scaling at present. Distributions of the number of rotations are very similar for both C- and IL-wall disruptions, while multi-turn mode rotations were observed in some cases. The I_p toroidal asymmetry amplitude seems to have no degradation with mode rotation frequency for both C- and IL-walls disruption data, therefore the dynamic amplification remains a serious issue since high amplitude multi-turn $m=n=1$ kink mode (which is responsible for the sideways forces) rotation can cause mechanical resonance of the machine components.

ACKNOWLEDGEMENT:
The authors would like to acknowledge M.F. Johnson for initial development of the JET disruption database and P. Noll for helpful discussions. This work, part-funded by the European Communities under the contract of Association between EURATOM/CCFE was carried out within the framework of the European Fusion Development Agreement. For further information on the contents of this paper please contact publications-officer@jet.efda.org. The views and opinions expressed herein do not necessarily reflect those of the European Commission. This work was also part-funded by the RCUK Energy Programme [grant number EP/I501045].

REFERENCE

[1]. Hender T C *et a*l 2007 *Nuclear Fusion* **47** S128

[2]. Sugihara M *et al* 2007 *Nuclear Fusion* **47** 337

[3]. Noll P. et al 1996 In Proceedings of the 19th Symposium on Fusion Technology Lisbon Vol. 1 p. 751

[4]. Riccardo V. *et al* 2000 *Nuclear Fusion* **40** 1805

[5]. Gerasimov S.N. *et al* 2010 *European Physical Society Conf. on Plasma Physics (Dublin, Ireland, 2010)* P4.121 http://ocs.ciemat.es/EPS2010PAP/pdf/P4.121.pdf

[6]. Hender T.C. *et al* 2010 EXS/10-3 *Proceedings of the 23rd IAEA FEC 2010* Daejeon Korea http://www-naweb.iaea.org/napc/physics/FEC/FEC2010/papers/exs_10-3.pdf

[7]. Zakharov L.E. *et al* 2012 *Physics of Plasmas* **19** 055703

[8]. Bachmann C. *et al* 2011 *Fusion Engineering and Design* **86**: 1915

[9]. Neyatani Y., Yoshino R. and Ando T. 1995 *Fusion Technol*ogy **28** 1634

[10]. Graenitz R.S. et al 1996 *Nuclear Fusion* **36** 545

[11]. Evans T.E. *et al* 1997 *Journal of Nuclear Materials* **241–243** 606

[12]. Gerasimov S.N. *et al* 2012 *European Physical Society Conf. on Plasma Physics (Stockholm, Sweden, 2012)* P5.074 ocs.ciemat.es/epsicpp2012pap/pdf/P5.074.pdf

[13]. Pautasso G. *et al* 2011 *Nuclear Fusion* **51** 043010

[14]. Gerhardt S.P. *et al* 2012 *Nuclear Fusion* **52** 063005

[15]. Schioler T. *et al* 2011 *Fusion Engineering and Design* **86**: 1963

[16]. Shafranov V.D. 1970 *Soviet Physics Technical Physics* **15** 175

[17]. Zakharov L. 2008 *Physics of Plasmas* **15** 062507

[18]. DeVries P.C. *et al* 2012 *Plasma Physics and Controlled Fusion* **54** 12403

[19]. Brezinsek S *et al* Fuel Retention Studies with the ITER-likeWall in JET, Contribution to the 24rd IAEA Fusion Energy Conference (San Diego 2012) EX/4-1, submitted to *Nucl. Fusion* (2012)

[20]. Riccardo V *et al* 2013 Fus. Eng. Des. (2013) http://dx.doi.org/10.1016/j.fusengdes.2013.01.084 *27th Symposium on Fusion Technology (SOFT-2012)* Liege

[21]. Romanelli F. *et al* 2012 *Proc. 24th Int. Conf. on Fusion Energy 2012 (San Diego, CA, 2012)* (Vienna: IAEA)

[22]. Strauss H.R. *et al* 2010 *Phys. Plasmas* **17** 082505

[23]. Lehnen M. *et al* 24th IAEA Fusion Energy Conference (FEC2012), EX/9-1, San Diego, submitted to *Nuclear Fusion*

[24]. Bachmann C. 2009 ITER report ITER_D_2DJ5AA v 2.7 https://user.iter.org/?uid=2DJ5AA)

[25]. Harris G.R. 1990 Comparisons of the current decay during carbon-bounded and beryllium bounded disruptions in JET JET-R (90) 07 http://www.iop.org/Jet/fulltext/JETR90007.pdf

[26]. McGrath R.T. and Kellman A.G. 1992 *Nuclear Fusion* **32** 2054

[27]. Granetz R.S. *et al* 2007 *Nuclear Fusion* **47** 1086

[28]. Last J. et al. 1999 Raising the JET Toroidal Field to 4 Tesla *JET-R (99) 10* http://www.iop.org/Jet/fulltext/JETR99010.pdf

[29]. Boozer A.H. 2012 *Physics of Plasmas* **19** 052508

[30]. Riccardo V. *et al* 2010 *Plasma Physics and Controlled Fusion* **52** 124018

[31]. Hender T.C. *et al* 2011 Report of the ITPA MHD Working Group 6 on Non-Axisymmetric Currents During VDEs *EFDA–JET–R(11)01* http://www.iop.org/Jet/fulltext/EFDR11001.pdf

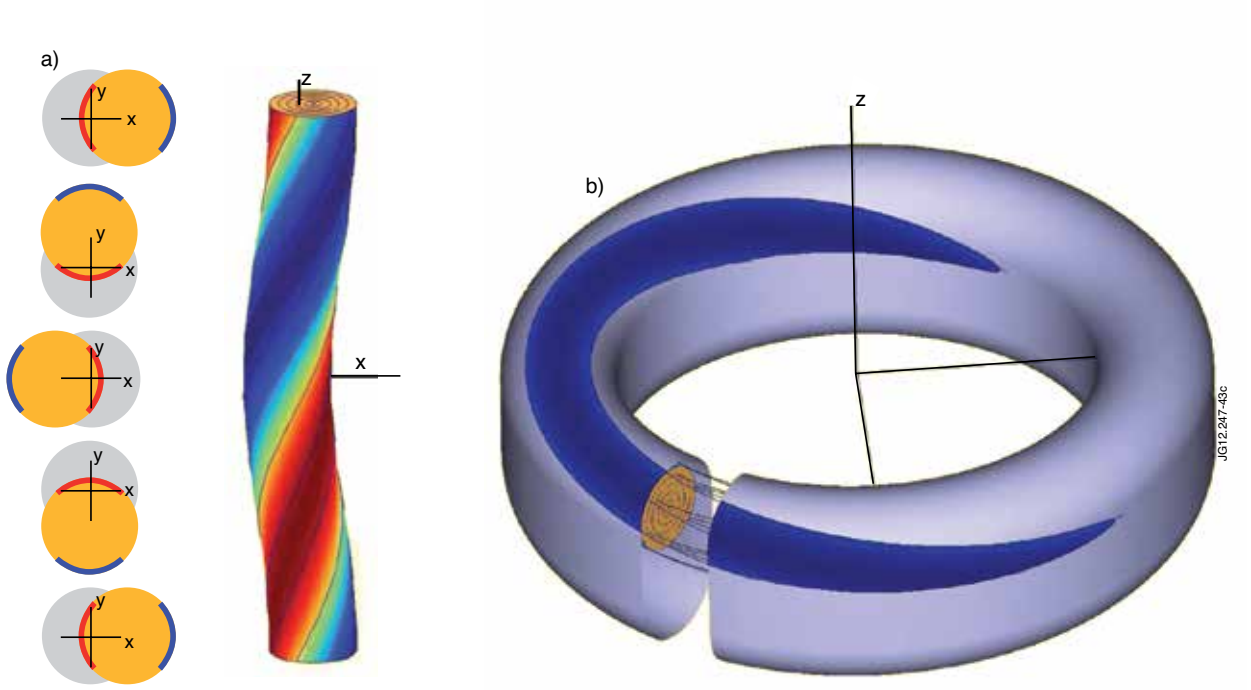

Figure 1: a) The bulged outer surface always carries the negative (blue) current, opposite to Ip. The bulged inner surface always carries the positive (red) current. b) Dark blue colour represents negative surfaces plasma current shared between vacuum vessel and plasma in VDE due to m=n=1 kink mode.

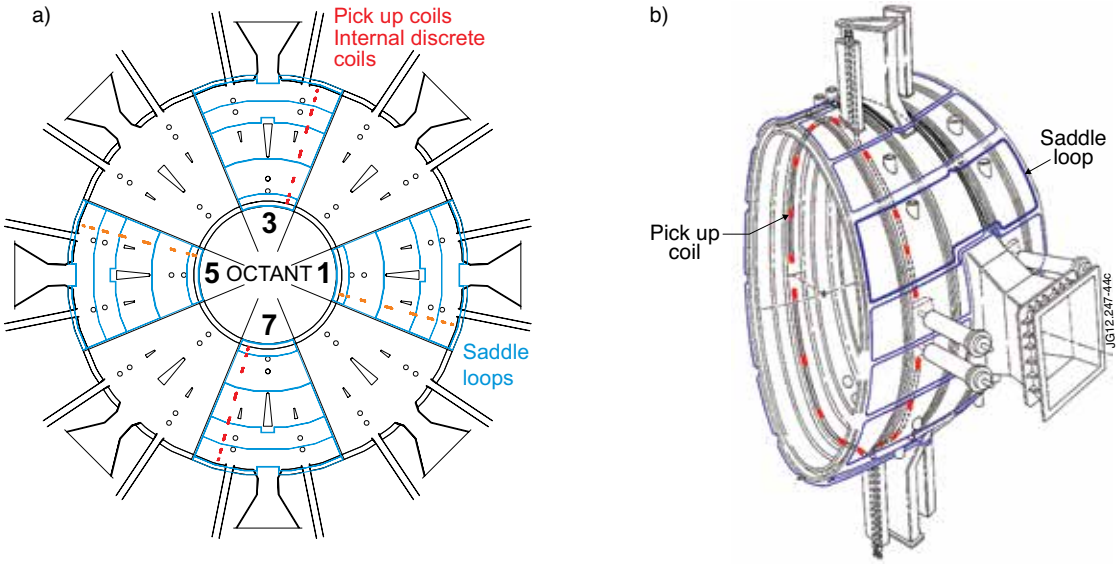

Figure 2: a) Plan view of JET vessel, showing the toroidal locations of the pick-up coils and saddles. b) JET vessel octant equipped with pick-up coils (named IDC) and saddle loops.

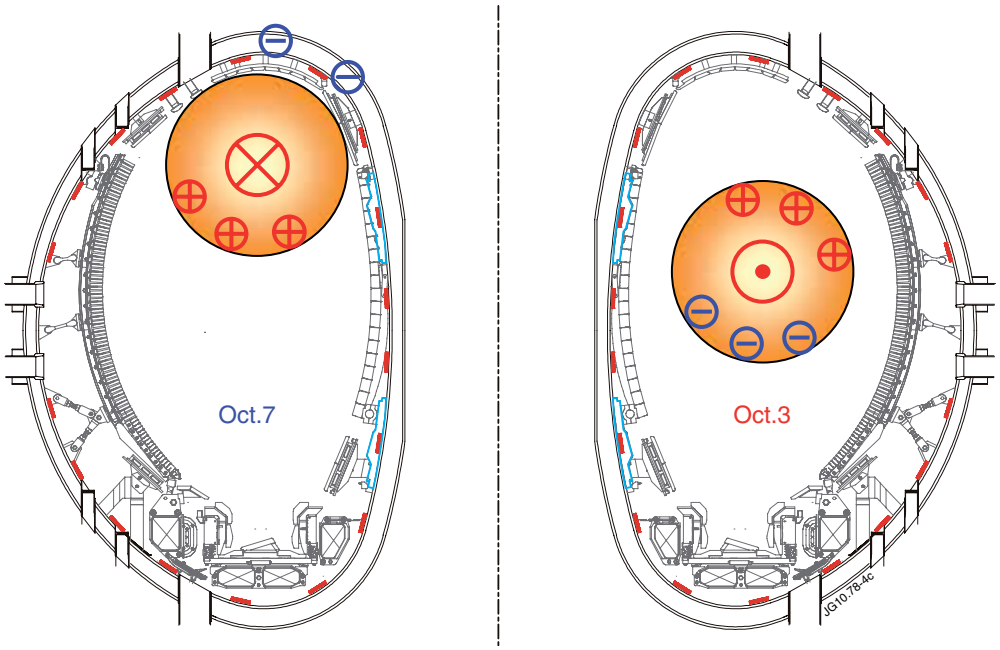

Figure 3: JET vessel cross-section and measured Ip asymmetry explanation. Negative surface plasma current flows on vessel in octant 7 and bypasses IDC contour. Restraining ring ribs are shown in light blue.

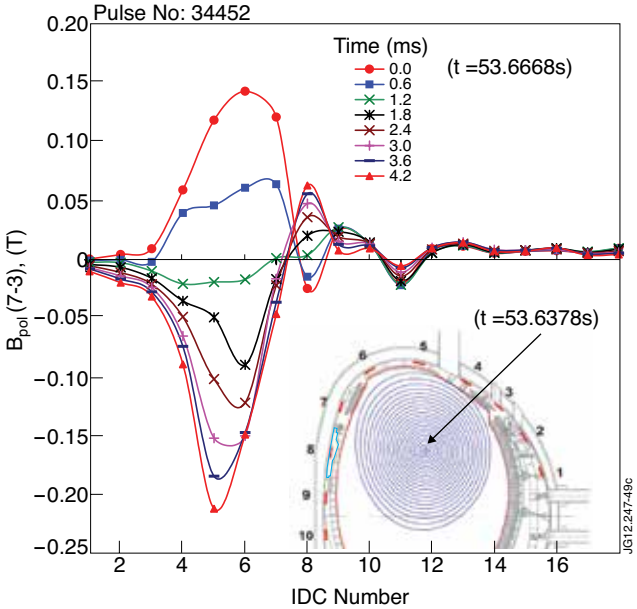

Figure 4: The asymmetry of the poloidal field measurements from IDCs. The insert shows the coil locations in the upper vessel (coils 10 to 18 are a mirror image); equilibrium reconstruction just before rise of the I_p asymmetry; restraining ring rib is shown in light blue.

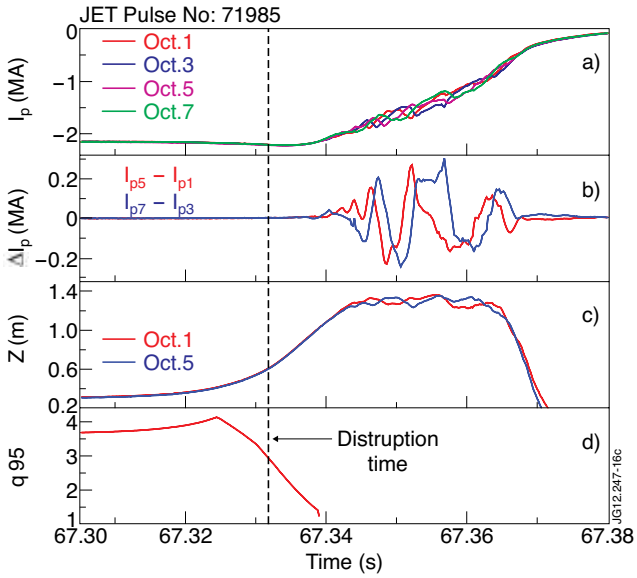

Figure 5: Waveforms of the measured asymmetries: a) plasma currents, b) I_p asymmetries, c) vertical plasma current centroid displacements and d) q_{95} edge safety factor. The vertical dashed line indicates the disruption time.

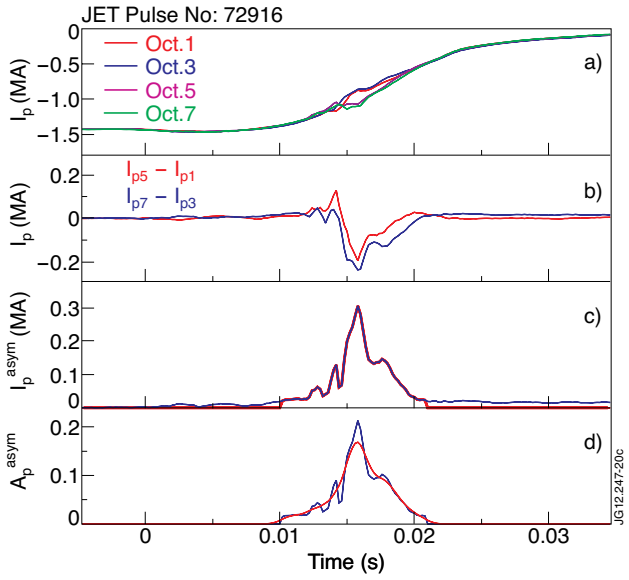

Figure 6: Waveforms of the measured asymmetries: a) plasma currents, b) I_p asymmetries, c) amplitude of the I_p asymmetries (blue – original, red – trimmed), d) normalized amplitude of the I_p asymmetries (blue – trimmed, red – smoothed). The time axis normalized to T_{dis}.

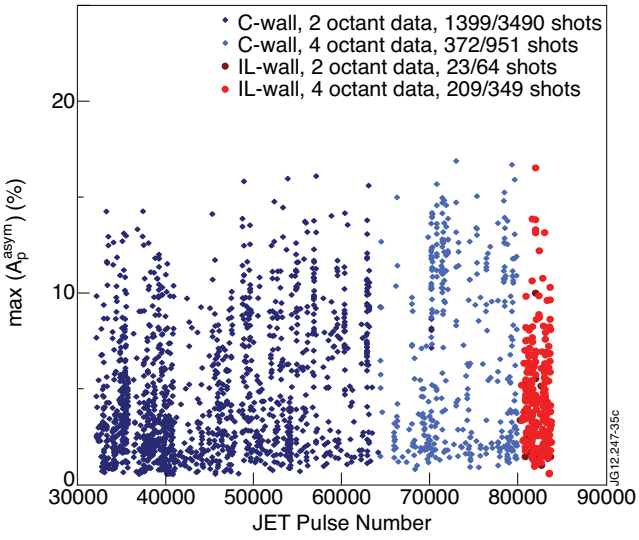

Figure 7: The amplitude of smoothed I_p asymmetry is <~17% of pre-disruptive I_p for whole range of the recorded disruptions.

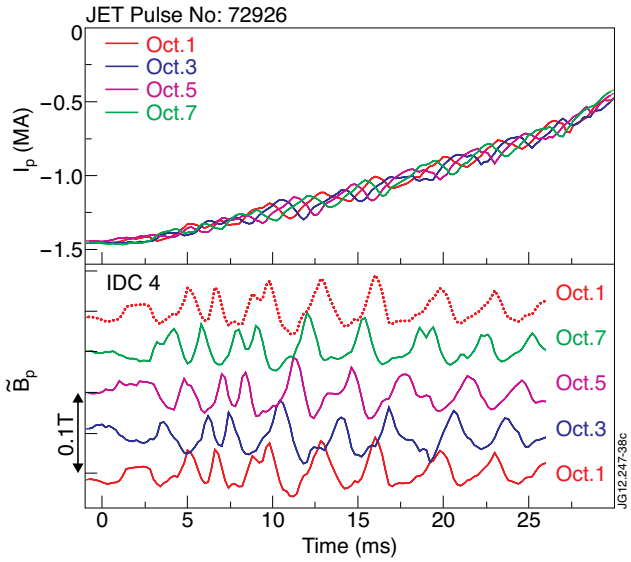

Figure 8: Poloidal field oscillations around torus show that I_p asymmetry is n = 1 dominated. Top – plasma currents, bottom – IDC 4 poloidal field variations around the torus. The time axis normalized to T_{dis}.

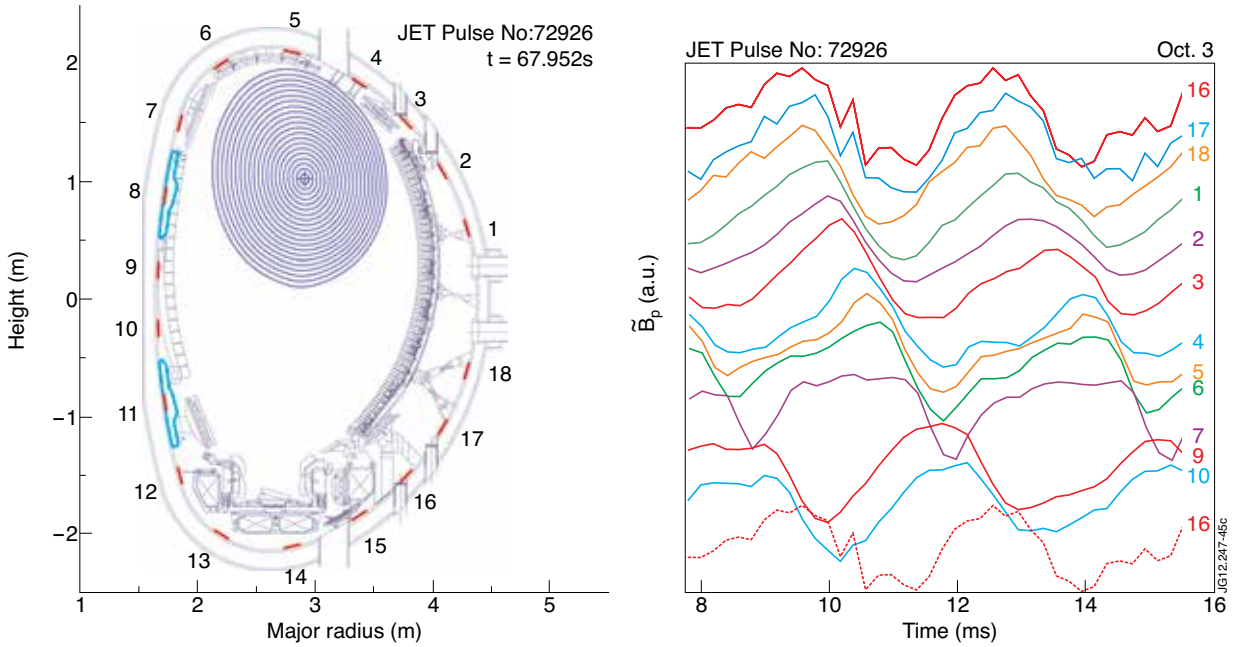

Figure 9: Left - equilibrium reconstruction just before rise of the I_p asymmetry; numbers show the IDCs. Right - poloidal field oscillations at octant 3 showing a dominantly m = 1 variation. The IDC numbers are indicated next to each waveform; the time axis normalized to T_{dis}.

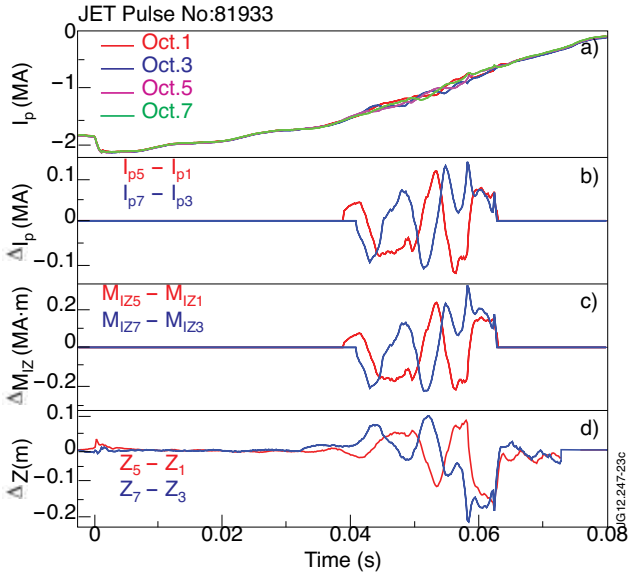

Figure 10: Waveforms of the measured asymmetries: a) plasma currents, b) I_p asymmetries, c) MIZ asymmetries, d) asymmetries of the vertical current centroid displacement. The time axis normalized to T_{dis}.

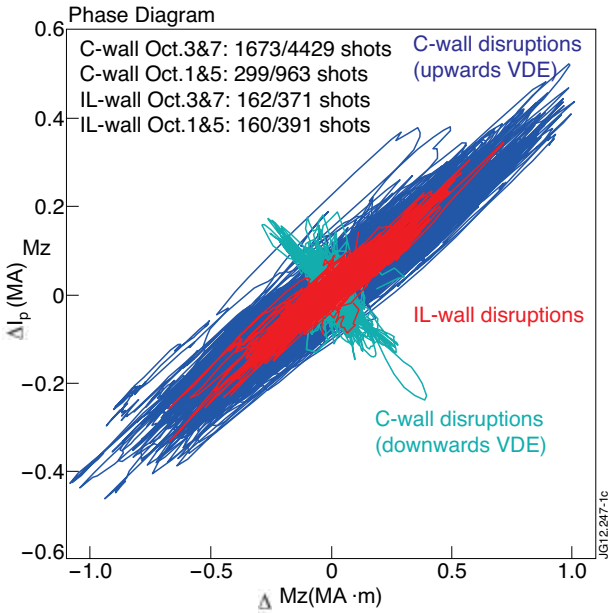

Figure 11: Phase relationship of the I_p and MIZ asymmetries: greater displacement leads to greater measured I_p asymmetry. The downwards VDE trajectories are orthogonal to upwards VDE trajectories because of the displacement polarity

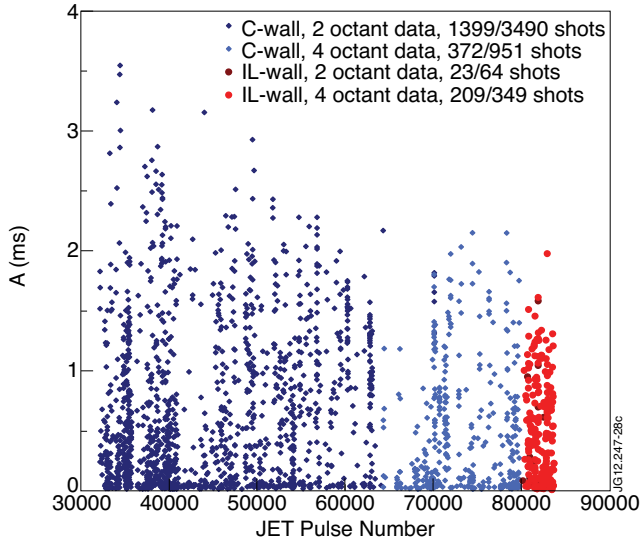

Figure 12: The integral of normalized I_p asymmetries for the entire disruption database.

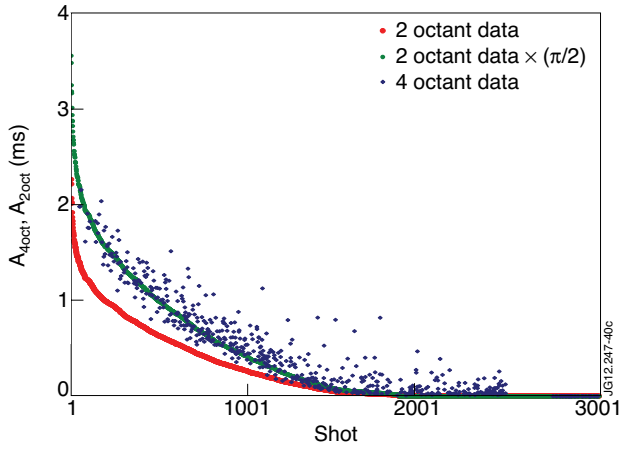

Figure 13: The entire 2 octant database (red), data for 4 octant shots (dark blue) where it exists, and $\pi A_{2oct}/2$ (green) - the data are sorted by descending size of A_{2oct}.

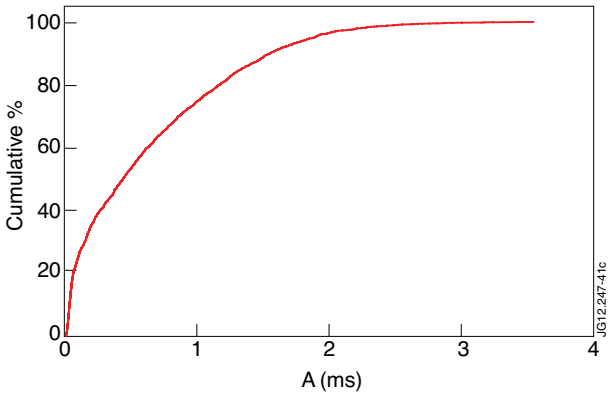

Figure 14: Cumulative % of shots with A less than a given value.

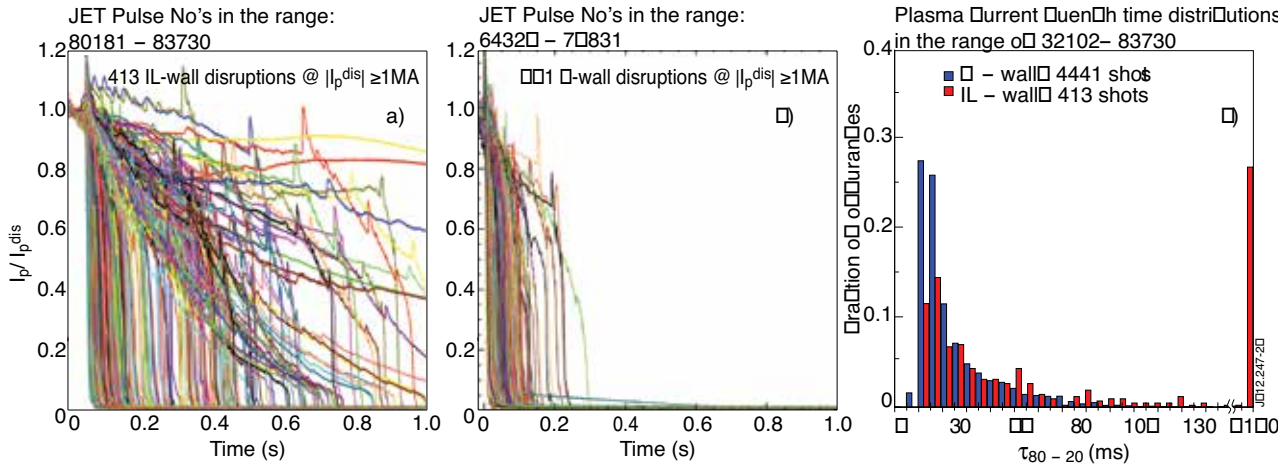

Figure 15: Normalised plasma current during disruptions: a) IL-wall, b) C-wall (only 951 last disruptions are shown) and c) their CQ time distributions for entire database; where $\tau_{80\text{-}20}$ is the CQ time extrapolated from time to quench from 80 to 20% of I_p^{dis}.

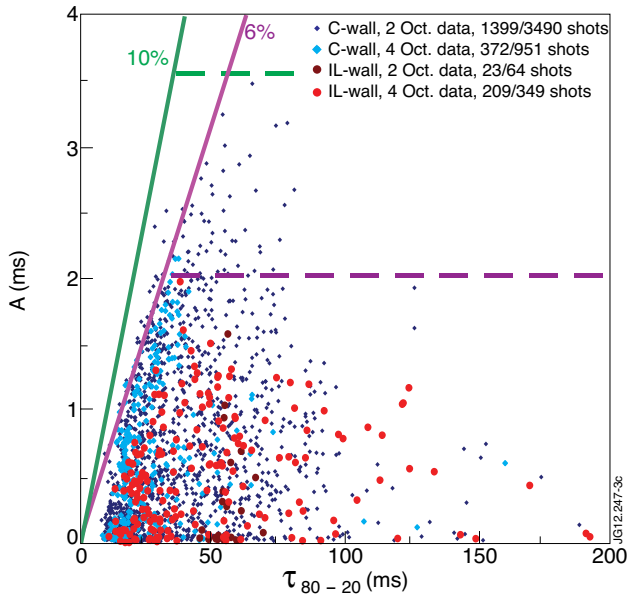

Figure 16: The severity of I_p asymmetries for C- and IL-walls.

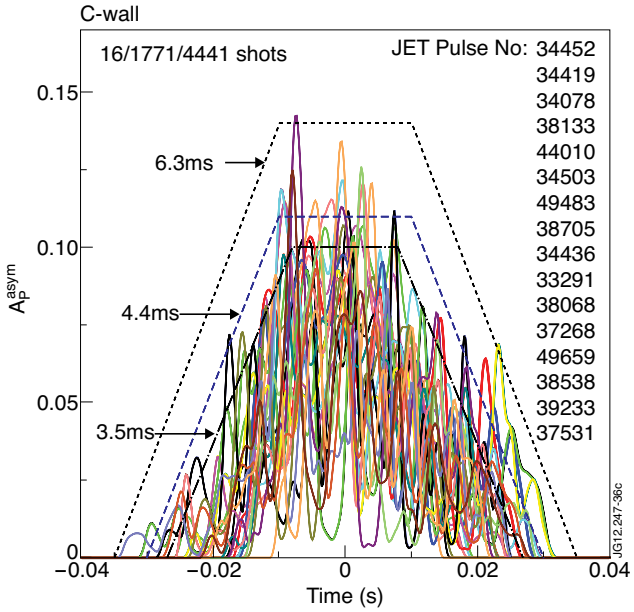

Figure 17: The smoothed normalised I_p asymmetries for 16 severest C-walls disruptions, where 1771/4441 is fraction of asymmetrical disruptions relative to whole C-wall database.

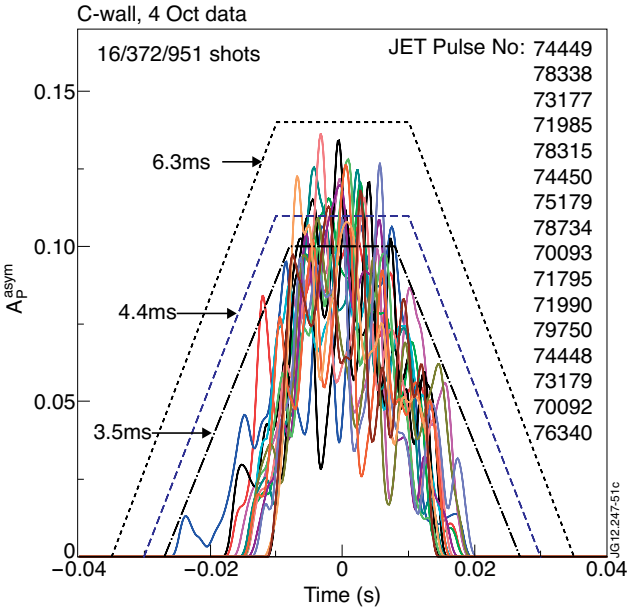

Figure 18: The smoothed normalised I_p asymmetries for 16 severest C-walls 4 octant data disruptions, where 372/951 is fraction of asymmetrical disruptions relative to C-wall 4 octant database.

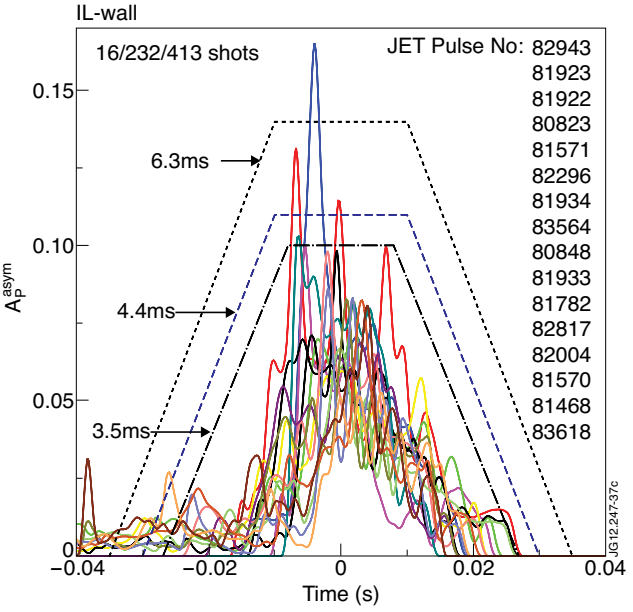

Figure 19: The smoothed normalised I_p asymmetries for 16 severest IL-walls disruptions, where 232/413 is fraction of asymmetrical disruptions relative to whole IL-wall database.

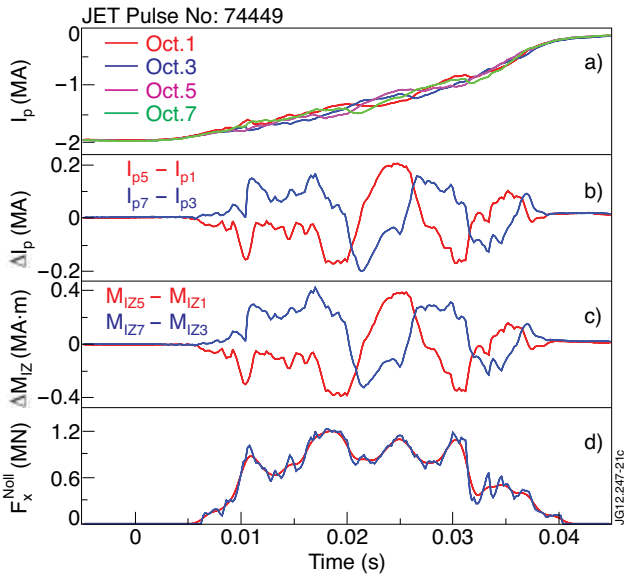

Figure 20: Waveforms of the measured asymmetries: a) plasma currents, b) asymmetries, c) MIZ asymmetries, d) F_x^{Noll} sideways force (blue – original, red – smoothed). The time axis normalized to T_{dis}.

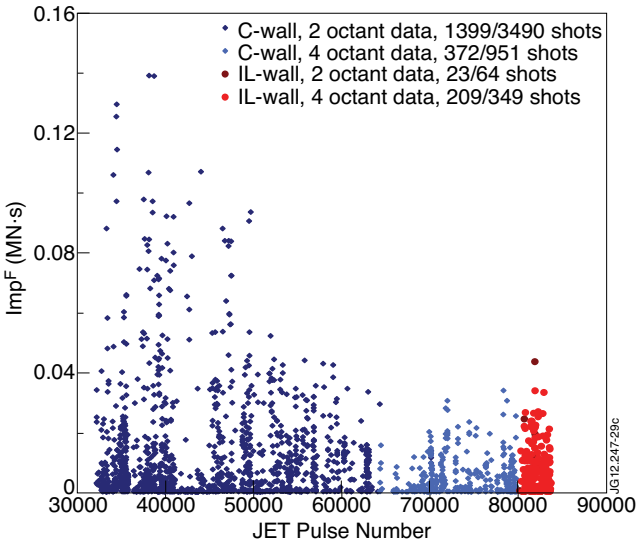

Figure 21: The sideways force impulse calculated using Noll's formula.

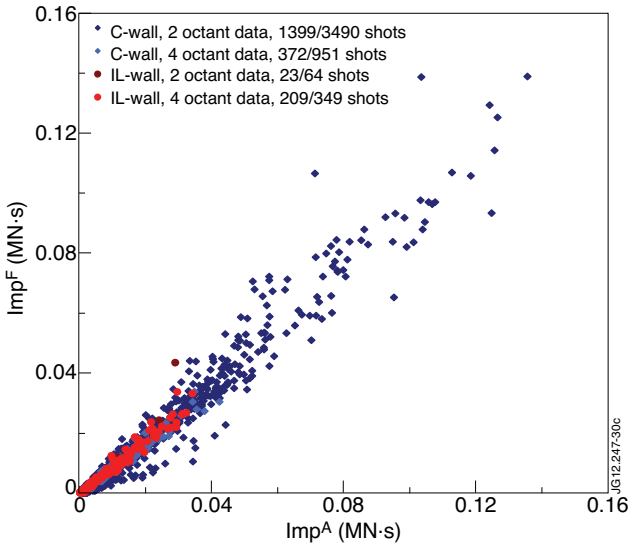

Figure 22: Relationship between sideways force impulse evaluated using the first current vertical moment (Imp^F) asymmetries and plasma current asymmetries(Imp^A) .

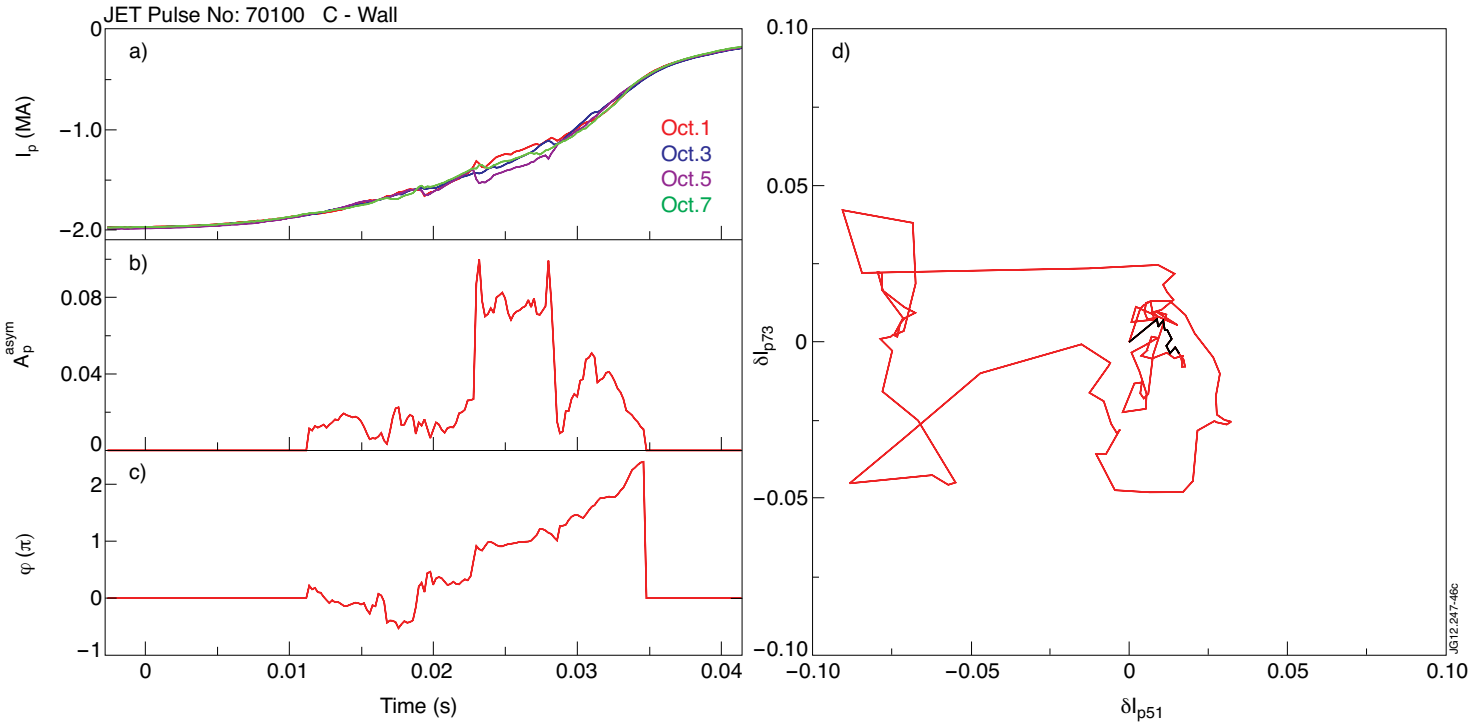

Figure 23: Example of the toroidally trapped motioned mode: a) plasma currents, b) normalized I_p asymmetry amplitude, c) mode toroidal angle (ϕ) and d) JET top view on trajectories of the tip of I_p asymmetry vector.

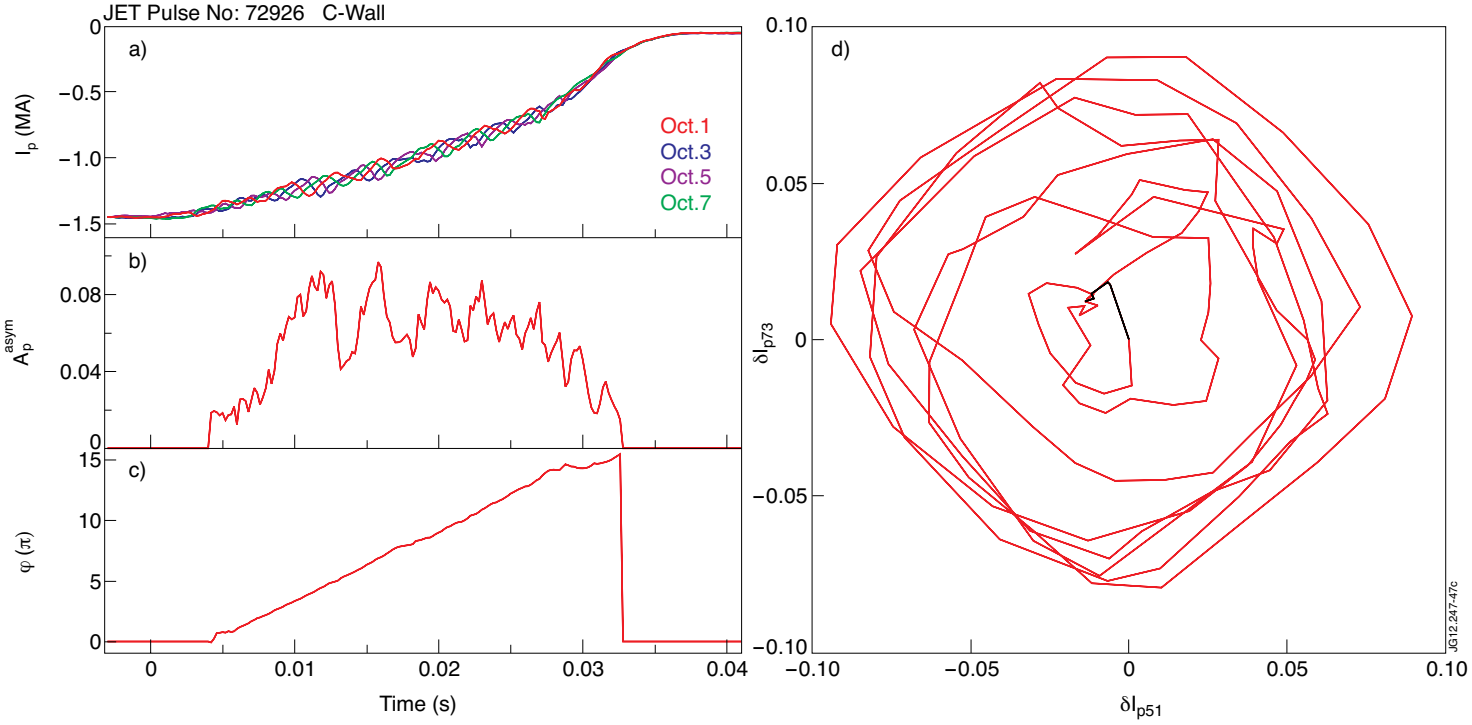

Figure 24: Example of the multi-turn fast rotation: a) plasma currents, b) normalized I_p asymmetry amplitude, c) mode toroidal angle (ϕ) and d) JET top view on trajectories of the tip of I_p asymmetry vector.

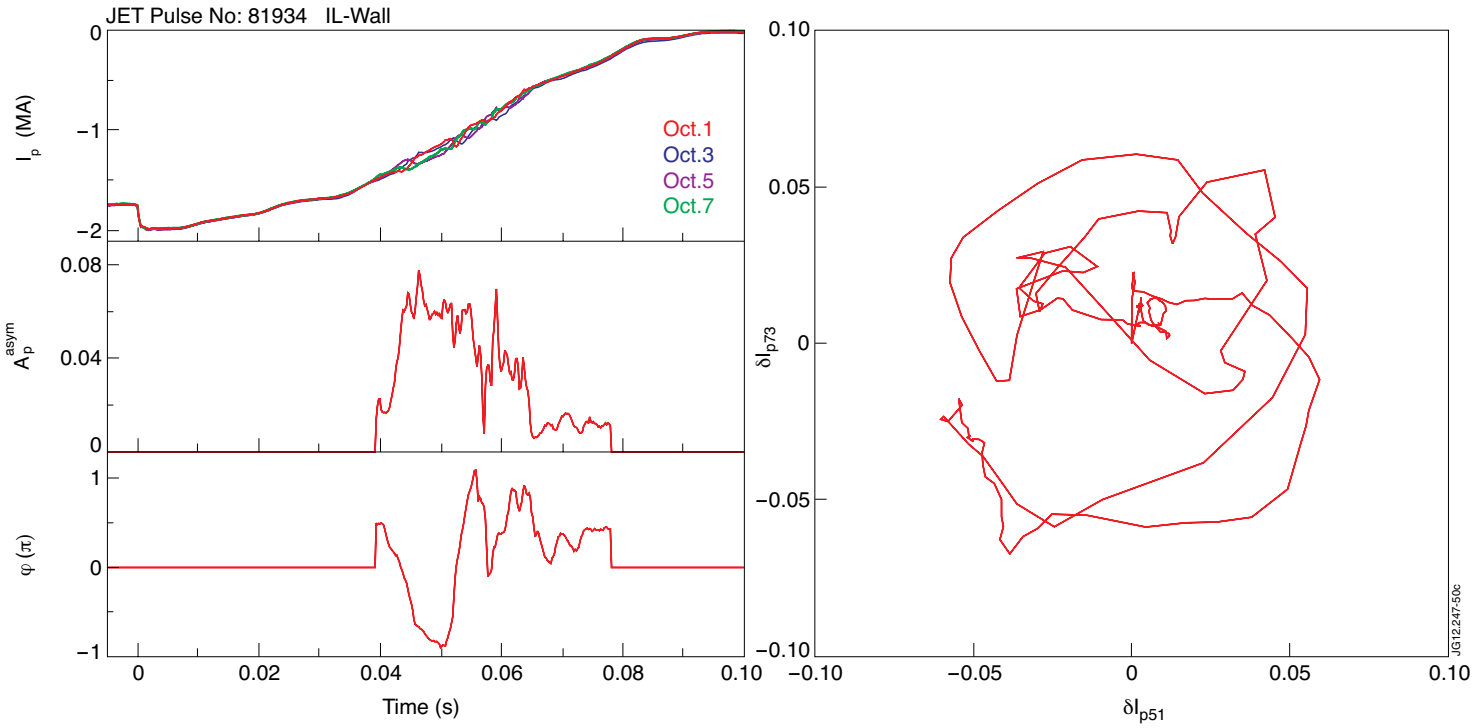

Figure 25: Example of rotation with reversal: a) plasma currents, b) normalized I_p asymmetry amplitude, c) mode toroidal angle (ϕ) and d) JET top view on trajectories of the tip of I_p asymmetry vector.

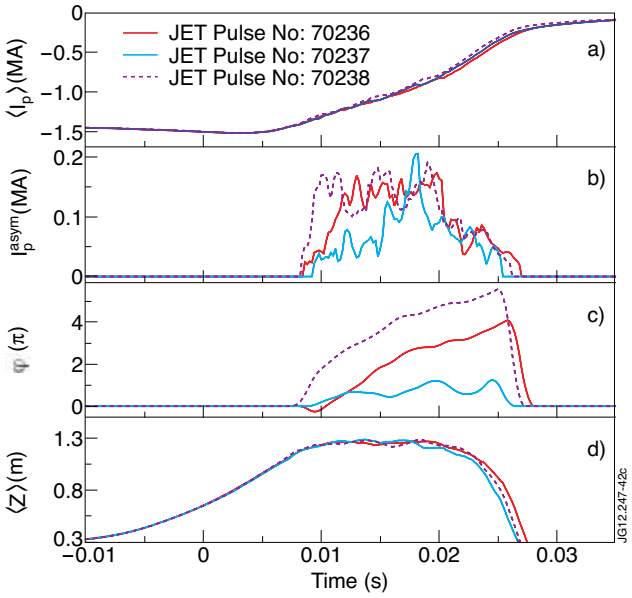

Figure 26: Examples of neighbouring pulses with similar plasma current and plasma current vertical displacement, in which (coincidentally) the earlier and the later pulses show coherent rotation and the intermediate pulse does not: a) toroidally averaged plasma current $\langle I_p \rangle$, b) I_p asymmetry amplitude, c) mode toroidal angle (ϕ) and d) toroidally averaged plasma current vertical centroid position $\langle Z \rangle$.

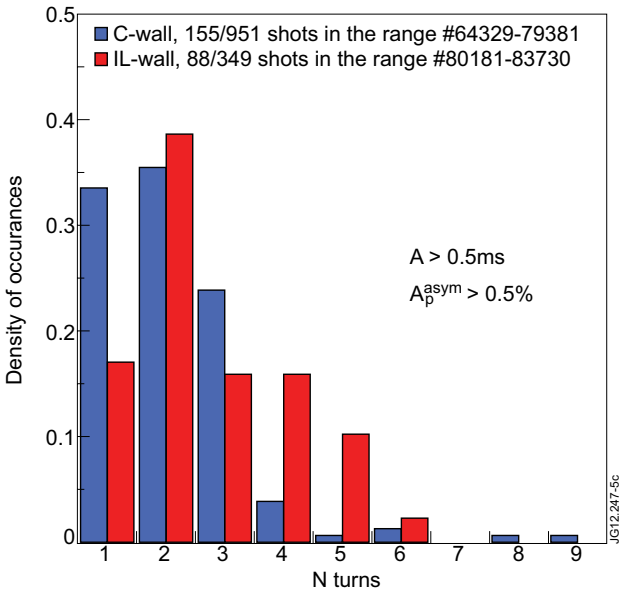

Figure 27: Distribution of the number of rotations.

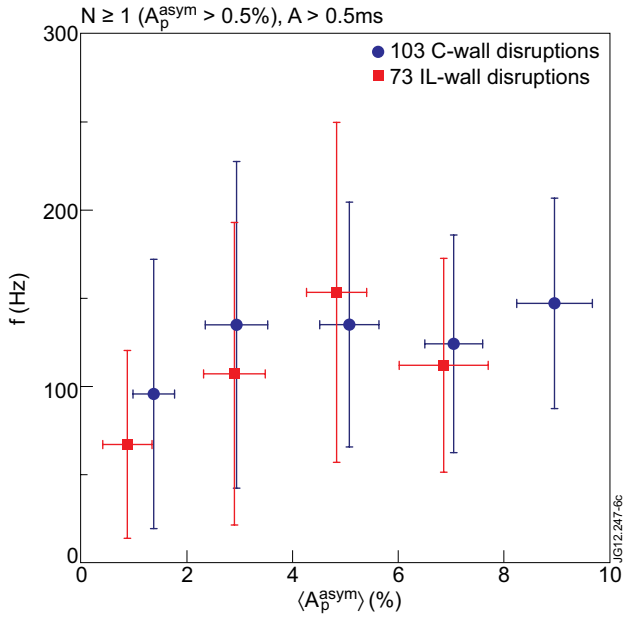

Figure 28: Variation of the "one turn" frequency versus average I_p asymmetry amplitude.

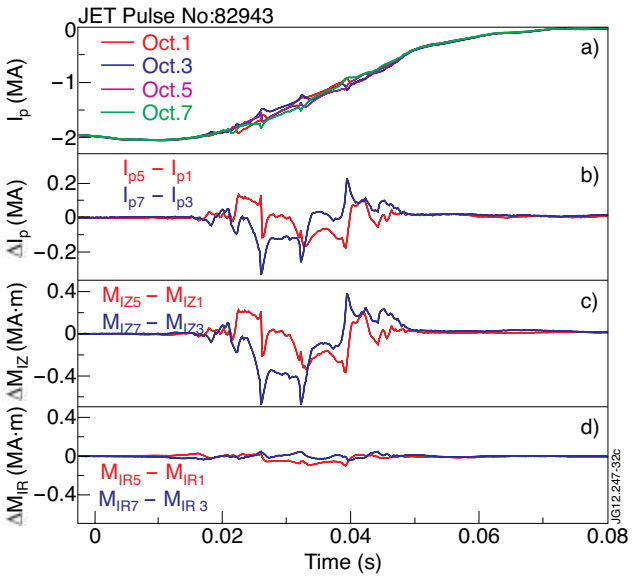

Figure 29: The magnetic diagnostic reported significantly smaller first radial plasma current moment variation (ΔM_{IR}) compare with ΔM_{IZ}. a) plasma currents, b) I_p asymmetries, c) M_{IZ} asymmetries, d) M_{IR} asymmetries. The time axis normalized to T^{dis}.